ChemComm

Intrinsic Volumetric Negative Thermal Expansion in the "Rigid" Calcium Squarate

Journal:	*ChemComm*
Manuscript ID	CC-COM-06-2021-003105.R1
Article Type:	Communication

COMMUNICATION

Intrinsic Volumetric Negative Thermal Expansion in the "Rigid" Calcium Squarate

Received 00th January 20xx,
Accepted 00th January 20xx

DOI: 10.1039/x0xx00000x

Zhanning Liu,[a] Zhe Wang,[a] Daofeng Sun,[a]* Xianran Xing[b]*

The calcium squarate with a rigid framework is found to exhibit volumetric negative thermal expansion (NTE) with the coefficient -9.51(5) × 10^{-6} K^{-1} and uniaxial zero thermal expansion (ZTE, -0.14(4) × 10^{-6} K^{-1}) over a wide temperature. Detailed comparison of the long-rang and local structure sheds light on that the anomalous thermal expansion originates from the transverse vibration of the bridging squarate ligand, although it has been tightly bonded by five calcium ions. We believe that this study can provide a deep insight into the origin of NTE and the structural flexibility of metal organic frameworks (MOFs).

Negative thermal expansion (NTE), as an intriguing abnormal phenomenon, has attracted considerable interests in the past two decades.[1] The emergence of NTE opens a pathway to the finely control of materials' thermal expansion behaviors to minimize thermal shock.[2] Besides, it can be utilized to modify related physical or chemical properties. For instance, Shao et al recently found that introducing NTE component $Y_2W_3O_{12}$ into the cathode of solid oxide fuel cell can greatly enhance its long-term electrode durability and oxygen reduction reaction activity.[3] Wang et al reported that using the NTE compounds as host lattices can effectively overcome the thermal quenching of upconversion fluorescence.[4-5] In spite of these promising applications, exploring novel NTE materials and elucidating the structural mechanism are ongoing challenges.

During the past three decades, great efforts have been devoted to explore NTE materials.[6] Till now, diverse materials have been reported, including alloys,[7-8] oxides,[6, 9] fluorides,[10-11] cyanides and metal-organic frameworks (MOFs).[12-13] For the open framework structured materials, the NTE is believed to be closely related to the structural flexibility. This also made MOFs an ideal platform to realize NTE.[14-15] The MOFs with "wine-rack" like motif can exhibit exceptional uniaxial NTE.[16-18] The helical structures can exhibit uniaxial NTE owing to the spring-like thermal motion.[19] However, these NTEs mainly originate from the thermal induced anisotropic geometric distortions. The uniaxial (or biaxial) NTE is usually overwhelmed by the larger positive thermal expansion (PTE) along perpendicular directions, leading to volumetric PTE. Alternatively, some carboxylate based MOFs can exhibit volumetric NTE, such as MOF-5,[20] HKUST-1,[21] MIL-68(In) and so on.[22-24] Unlike the above-mentioned flexible MOFs, on the one hand, these structures are rigid enough to forbid obvious geometric distortion. On the other hand, the "knee-cap" like rotation of carboxylate group can pull two terminal metal ions closer, leading to the generation of NTE.[25-26] However, in the absence of carboxylate like unit, the "rigid unit modes" that are responsible for NTE can hardly be supported.[27] For example, the methyl-imidazole bridged ZIF-8 shows normal PTE,[28] although the imidazolate ring is allowed to rotate.[29]

Recently, the calcium squarate (termed as Ca_sq, also known as UTSA-280) was reported to be much more rigid than carboxylate MOFs and ZIFs. In this structure, the rigid squarate unit is directly bonded by five calcium atoms without any additional buffering bridges, which was believed can effectively restrain the ligand rotation. Benefitting from the framework rigidity and suitable pore size, it shows excellent gas separation properties.[30] In this work, we report, for the first time, the squarate group in Ca-sq can actually exhibit strong local transverse vibrations to result in a volumetric NTE. The underlying mechanism is explored by joint analyses of high resolution synchrotron based powder X-ray diffraction, single crystal X-ray diffraction, atomic pair distribution function (PDF) and Raman spectrum.

The Ca_sq was synthesized according to previous reference.[30-31] The synthesized sample possesses colourless needle shaped morphology (Figure S1). Element analyses indicates the formula $[Ca(C_4O_4)H_2O]\cdot H_2O$, (found Ca: 20.91%; C: 24.70%; H: 2.61%; O: 51.78%), which is in good agreement with the reported result.[31] The Ca_sq crystalizes in the tetragonal

[a] *School of Materials Science and Engineering, China University of Petroleum (East China), Qingdao, Shandong, 266580, China.*
[b] *Beijing Advanced Innovation Center for Materials Genome Engineering, Institute of Solid State Chemistry, University of Science and Technology Beijing, Beijing, 100083, China.*
Electronic Supplementary Information (ESI) available: [details of any supplementary information available should be included here]. See DOI: 10.1039/x0xx00000x

phase with the space group *I*-42*d* (Figure 1a and Table S1). Owing to the non-centrosymmetric crystal structure, it exhibits a mediate second harmonic generation (SHG) response of ~ 0.8 × KH_2PO_4 (Figure S2). In this structure, the calcium ion is coordinated by seven oxygen atoms from five squarate ligands and one water molecule (Figure 1b). There are square shaped 1D channels along the *c*-axis. For the as-synthesized compound, the channel is occupied by guest water molecules, as confirmed by the thermogravimetric analysis (TGA, Figure S3). The guest water molecules can be removed by thermal treatment (~370 K) without breaking the framework structure. Furthering increasing temperature to ~550 K causes the loss of coordination water molecules, leading to the collapse of framework. Since the guest desorption may influence the intrinsic properties of host framework,[32-33] the sample was fully activated before measurements.

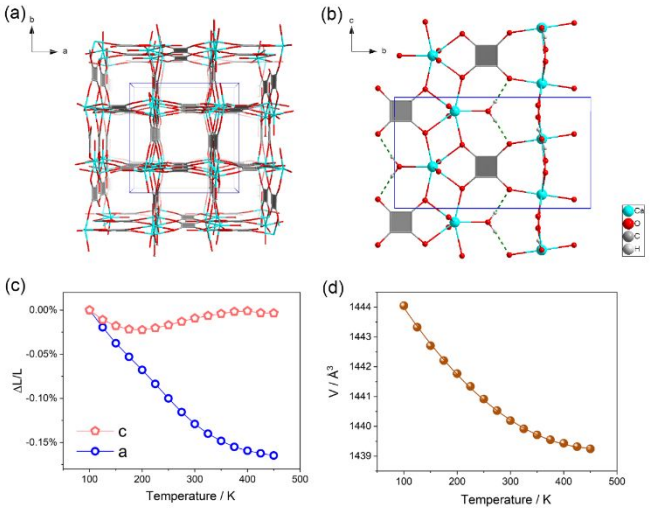

Figure 1 Crystal structure of Ca_sq viewing along *c*- (a) and *a*- (b) axis. (c) Relative lattice parameter changes of the activated Ca_sq. (d) Temperature dependent unit cell volume. The error bars are smaller than the symbols.

In situ high-resolution synchrotron powder X-ray diffraction (HR-SXRD) measurements (Figure S4) and Rietveld refinements (Figure S5) were performed to evaluate the thermal expansion properties of Ca_sq. With increasing temperature, no phase transition occurred. The extracted lattice parameters from Rietveld refinements are shown in Figure 1c, d and Table S2. With increasing temperature (100~450 K), the lattice parameter *a* decreases monotonically while the parameter *c* nearly remains unchanged. The corresponding linear coefficients of thermal expansion (CTEs) for *a*- and *c*-axis are -4.71(2) × 10^{-6} K^{-1} and -0.14(4) × 10^{-6} K^{-1}, respectively. Noticeably, the magnitude of CTE along *c*-axis is smaller than most of the reported zero thermal expansion (ZTE) materials (Table S3). A volumetric NTE was also observed and the corresponding CTE is -9.51(5) × 10^{-6} K^{-1} (Figure 1d), which is close to the value of the well-known ScF_3 (-9.6× 10^{-6} K^{-1}, 300~800 K).[10, 34]

To elucidate the origin of NTE, single crystal X-ray diffraction (SCXRD) analyses were performed and the detailed bond length changes are shown in Figure 2. In this structure, the center of squarate occupies a special Wyckoff site *8d* and there is a 2-fold rotation axis along the *a*-axis. The coordination water molecule forms hydrogen bond with the O2 atom of squarate with the H…O distance 1.91(4) Å (Figure 2a). Upon heating, the coordination bond Ca-O1 expands from 2.413(1) to 2.416(1) Å, while the bond Ca-O2 contracts from 2.316(1) to 2.313(1) Å (Figure 2b). The distances between Ca and C atoms show similar trends (Figure 2c). Noticeably, within the squrate ligand, the C-C bonds show little changes (Figure 2e), while the C-O bonds contract steeply (Figure 2d), especially the C2-O2 bond that contracts from 1.253(3) to 1.245(3) Å.

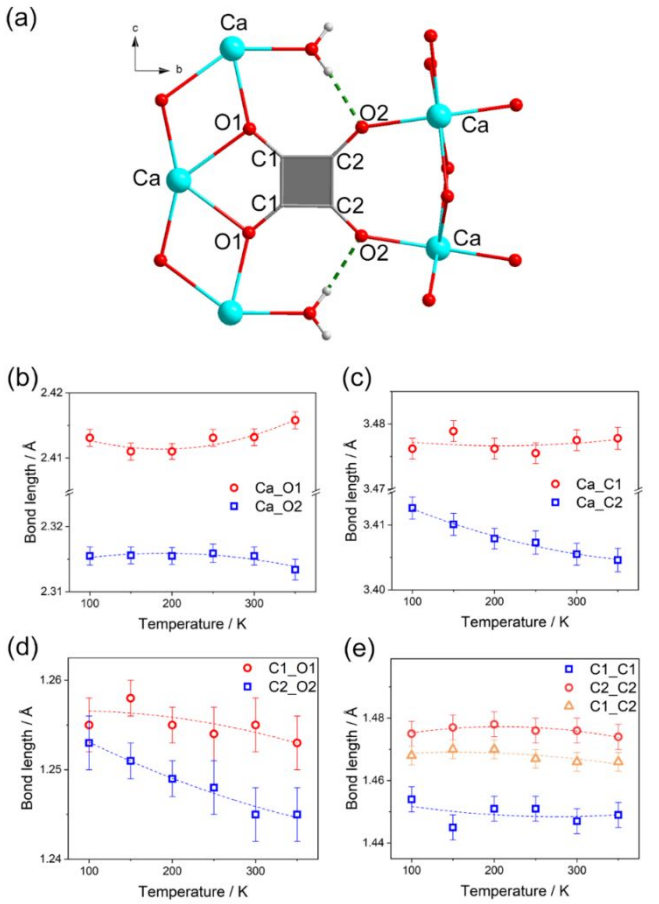

Figure 2 (a) Local coordination mode of the Ca_sq and the definition of atom names. The dashed green lines represent the hydrogen bonds. Temperature dependent bond lengths obtained from SCXRD, Ca-O (b), Ca..C (c), C-O (d) and C-C (e).

It should be noted that, owing to the anharmonic nature of potential energy, the distance between two directly bonded atoms generally expands upon heating.[1, 35] Some previous references have demonstrated that the observed unphysical bond contractions may be caused by the dynamic vibrations and crystallographic symmetry constrains.[12, 34, 36-37] Based on this, in situ synchrotron based atomic PDF analyses were carried out to investigate the "real" local structural changes (Figure 3a). Although high resolution data has been collected (Q_{max} = 22 $Å^{-1}$), there are still peak overlaps (C1-O1 with C2-O2, C1-C1 with

C2-C2 *etc*), which may be caused by the approximate bond lengths and low scattering power of carbon and oxygen atoms. Fortunately, the trends of local structural changes can be easily identified by merging the similar bond lengths. In the high *r* region, the peaks are mainly dominated by the Ca…Ca correlations (Figure 3b). Upon heating, the peaks that correspond to the Ca-Ca correlations (~7.7, ~8.5, ~10.3, ~11.5 Å *etc*) broaden quickly compared with the hydrated one (Figure S6), inferring the flexibility of Ca_sq.[11, 38] The partial PDF patterns below 4 Å are shown in Figure 3c. It can be clearly seen that the squarate ligand (C-C and C-O correlations) shows little changes upon heating, which is consistent with the rigidity feature of aromatic units.[39] The Ca-O correlation shows obvious thermal expansion. Noticeably, the C-O and Ca-O changes are contrary to the "apparent" bond length changes obtained from Bragg analyses (Figure 2b). As for the none directly bonded Ca…C, it continuously shrinks upon heating. Based on the difference between the "true" and "apparent" bond length changes, it is reasonable to believe that there are strong dynamic vibrations between the squarate ligands and calcium ions. In the longer range (Figure 3d), the peak at ~7.7 Å corresponds to the Ca…Ca distance along *c*-axis, which equals to the lattice parameter *c*. Upon heating, the peak position shows little changes but with an obvious broaden. This is consistent with the observed ZTE behavior. The peak at ~8.5 Å corresponds the diagonal Ca…Ca distance across the square channel within the *ab* plane. With increasing temperature, it shifts toward lower *r* values, indicating NTE. This trend agrees well with the Bragg analysis results (Figure 1c).

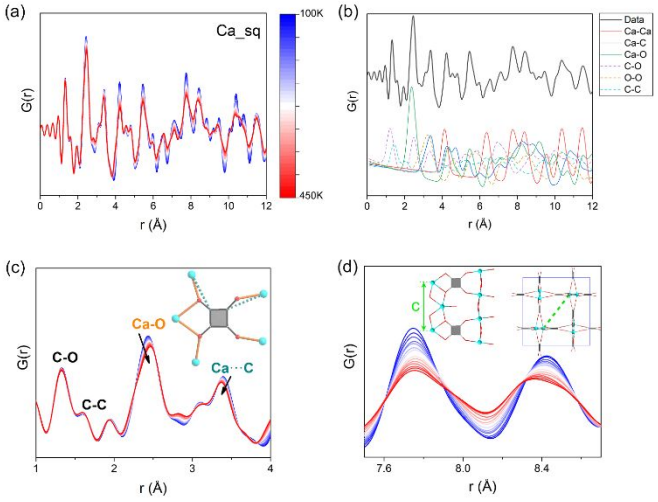

Figure 3 (a) Variable temperature PDF patterns from 100 to 450 K. (b) The experimental PDF pattern at 300 K (black) and calculated partial PDF that corresponds to Ca-Ca (red), Ca-C (blue), Ca-O (green), C-O (purple dashed), O-O (brown) and C-C (cyan dashed). (c) Partial PDF that below 4 Å. The PDF peaks labelled by different colours are depicted in the upper inset by the same colour bonds. (d) Partial PDF in the range 7.5~8.7 Å, the insets correspond to the Ca-Ca correlations with the length ~7.7 Å (left) and 8.5 Å (right).

To shed light on the dynamic behavior of the framework, temperature dependent anisotropic atomic displacement parameters (ADPs) were analysed. As shown in Figure 4a, the thermal ellipsoids of carbon and oxygen are quite elongated mainly perpendicular to the squarate plane. Detailed comparison of the rate of changes of ADPs with temperature (*dU/dT*) clearly demonstrates that the squarate ligand tends to exhibit preferred transverse vibrations upon heating.[21, 40] Raman spectrum, an effective approach to detect lattice vibrations, was used to prove the proposed thermal motion.[41-42] Owing to the detector cutoff, the spectra were collected from 53 cm^{-1}. Upon heating (Figure 4c and d), most of the Raman modes show normal soften except the mode ~57 cm^{-1}. The anomalous stiffen of this mode indicates that it may contributes to the generation of NTE.[43-44] Further DFT calculations were performed to investigate the corresponding Raman modes. The experimental spectrum is consistent with the calculated result (Figure 4b). The DFT calculations reveal that the mode at ~57 cm^{-1} corresponds to the skipping-rope vibration. Noticeably, there is another type of transverse vibration mode in the lower energy region ~27 cm^{-1}, which corresponds to the antiparallel vibration, similar with the similar with the Prussian blue analogues and MOF-5.[12, 27] We have to admit that it's hard to distinguish which mode makes a dominant contribution to the NTE. However, according to the *dU/dT* values (O2 > O1 > C2 > C1), it can be concluded that the oxygen atoms in squarate exhibit significant stronger transverse vibration than the carbon atoms and the magnitude of O2 is larger than that of the O1. This is in agreement with the observed apparent contraction of the C2-O2 and Ca-O2 lengths. The different flexibility of O1 and O2 may be caused by their different coordination mode. The O1 is fixed tighter by two calcium ions while the O2 is fixed only by a calcium ion and a weaker hydrogen bond. Since the hydrogen bond is usually more sensitive to temperature, it can largely enhance the flexibility of O2.

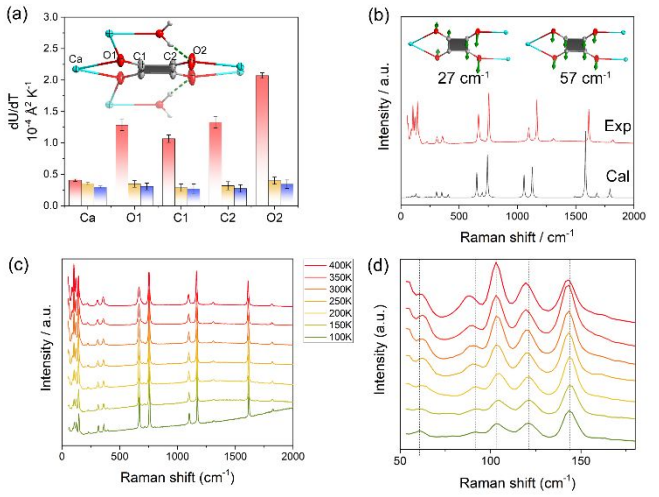

Figure 4 (a) Rate of changes of ADPs with temperature. The values are given for the three ADP axes: major (red), intermediate (yellow) and minor axes (blue). The upper inset shows 50% probability thermal ellipsoids of Ca_sq that obtained from the refinement of SCXRD data (300 K). (b) The experimental (red) and calculated (black) Raman spectra of Ca_sq. The insets illustrate the low-energy transverse vibration at 27 cm^{-1} (left) and 57 cm^{-1} (right). Variable temperature Raman spectra of Ca_sq (c) and the zoomed low frequency region.

In summary, we here found that the NTE can exist in rigid MOFs that are lack of carboxylate like buffering units. The Ca_sq shows a rare volumetric NTE accompanied with a uniaxial ZTE. A comprehensive study of the "apparent" and "real" bond length changes revealed that the anomalous thermal expansion originates from the transverse vibration of the bridging squarate ligand, although it has been tightly bonded. The related low-energy vibration modes were also confirmed by the Raman spectrum. This study can not only deepen our knowledge of the origin of NTE but also provide a guidance for the rational design and exploration of novel NTE materials.

This research was supported by National Key R&D Program of China (2020YFA0406202), the National Natural Science Foundation of China (grant nos. 22090042, 21731001 and 22005340), the Fundamental Research Funds for the Central Universities (20CX06047A), Taishan Scholar Foundation (ts201511019) and Development Projects of Shandong Province (Grant 2019JZZY010331). The HR-SXRD experiments were performed with the approval of SPring-8 (proposal NO. 2018B1306). This research also used resources of the Advanced Photon Source, a U.S. Department of Energy (DOE) Office of Science User Facility operated for the DOE Office of Science by Argonne National Laboratory under contract no. DE-AC02-06CH11357. The authors also acknowledge the assistance of beamline scientists at 11-ID-C of Advanced Photon Sources.

Conflicts of interest

There are no conflicts to declare.

Notes and references

1 J. Chen, L. Hu, J. Deng and X. Xing, *Chem. Soc. Rev.*, 2015, **44**, 3522-3567.
2 K. Takenaka, *Sci. Technol. Adv. Mater.*, 2012, **13**, 013001.
3 Y. Zhang, B. Chen, D. Guan, M. Xu, R. Ran, M. Ni, W. Zhou, R. O'Hayre and Z. Shao, *Nature*, 2021, **591**, 246-251.
4 H. Zou, X. Yang, B. Chen, Y. Du, B. Ren, X. Sun, X. Qiao, Q. Zhang and F. Wang, *Angew. Chem. Int. Ed.,* 2019, **58**, 17255-17259.
5 B. Ren, B. Chen, J. Zhao, Y. Guo, X. Zhang, X. Chen, Y. Du, Z. Deng, G. Zhu and F. Wang, *Chem. Mater.*, 2021, **33**, 158-163.
6 T. Mary, J. Evans, T. Vogt and A. Sleight, *Science*, 1996, **272**, 90-92.
7 M. Van Schilfgaarde, I. Abrikosov and B. Johansson, *Nature*, 1999, **400**, 46-49.
8 Y. Song, J. Chen, X. Liu, C. Wang, J. Zhang, H. Liu, H. Zhu, L. Hu, K. Lin, S. Zhang and X. Xing, *J. Am. Chem. Soc.,* 2018, **140**, 602-605.
9 J. Chen, X. Xing, C. Sun, P. Hu, R. Yu, X. Wang and L. Li, *J. Am. Chem. Soc.*, 2008, **130**, 1144-1145.
10 B. K. Greve, K. L. Martin, P. L. Lee, P. J. Chupas, K. W. Chapman and A. P. Wilkinson, *J. Am. Chem. Soc.*, 2010, **132**, 15496-15498.
11 L. Hu, J. Chen, J. Xu, N. Wang, F. Han, Y. Ren, Z. Pan, Y. Rong, R. Huang, J. Deng, L. Li and X. Xing, *J. Am. Chem. Soc.* 2016, **138**, 14530-14533.
12 K. W. Chapman, P. J. Chupas and C. J. Kepert, *J. Am. Chem. Soc.,* 2005, **127**, 15630-15636.
13 Y. Wu, V. K. Peterson, E. Luks, T. A. Darwish and C. J. Kepert, *Angew. Chem. Int. Ed.*, 2014, **126**, 5275-5278.
14 Z. Liu, Q. Gao, J. Chen, J. Deng, K. Lin and X. Xing, *Chem. Commun.*, 2018, **54**, 5164-5176.
15 Z. Liu, L. Zhang and D. Sun, *Chem. Commun.*, 2020, **56**, 9416-9432.
16 L. D. DeVries, P. M. Barron, E. P. Hurley, C. Hu and W. Choe, *J. Am. Chem. Soc.*, 2011, **133**, 14848-14851.
17 H. Zhou, Y. Zhang, J. Zhang and X. Chen, *Nat. Commun.*, 2015, **6**, 6917.
18 F. X. Coudert and J. D. Evans, *Coord. Chem. Rev.*, 2019, **388**, 48-62.
19 Z. Liu, C. Liu, Q. Li, J. Chen and X. Xing, *Phys. Chem. Chem. Phys.*, 2017, **19**, 24436-24439.
20 D. Dubbeldam, K. S. Walton, D. E. Ellis and R. Q. Snurr, *Angew. Chem. Int. Ed.,* 2007, **119**, 4580-4583.
21 Y. Wu, A. Kobayashi, G. J. Halder, V. K. Peterson, K. W. Chapman, N. Lock, P. D. Southon and C. J. Kepert, *Angew. Chem. Int. Ed.*, 2008, **47**, 8929-8932.
22 Z. Liu, Q. Li, H. Zhu, K. Lin, J. Deng, J. Chen and X. Xing, *Chem. Commun.,* 2018, **54**, 5712-5715.
23 M. J. Cliffe, J. A. Hill, C. A. Murray, F.-X. Coudert and A. L. Goodwin, *Phys. Chem. Chem. Phys.,* 2015, **17**, 11586-11592.
24 Z. Liu, R. Ma, J. Deng, J. Chen and X. Xing, *Chem. Mater.,* 2020, **32**, 2893-2898.
25 N. Lock, Y. Wu, M. Christensen, L. J. Cameron, V. K. Peterson, A. J. Bridgeman, C. J. Kepert and B. B. Iversen, *J. Phys. Chem. C,* 2010, **114**, 16181-16186.
26 C. Serre, C. Mellot-Draznieks, S. Surblé, N. Audebrand, Y. Filinchuk and G. Férey, *Science*, 2007, **315**, 1828-1831.
27 W. Zhou, H. Wu, T. Yildirim, J. R. Simpson and A. R. Hight Walker, *Phys. Rev. B.*, 2008, **78**, 054114.
28 A. F. Sapnik, H. S. Geddes, E. M. Reynolds, H. H.-M. Yeung and A. L. Goodwin, *Chem. Commun.*, 2018, **54**, 9651-9654.
29 D. Fairen-Jimenez, S. A. Moggach, M. T. Wharmby, P. A. Wright, S. Parsons and T. Duren, *J. Am. Chem. Soc.*, 2011, **133**, 8900-8902.
30 R. Lin, L. Li, H. Zhou, H. Wu, C. He, S. Li, R. Krishna, J. Li, W. Zhou and B. Chen, *Nat. Mater.*, 2018, **17**, 1128-1133.
31 C. Robl and A. Weiss, *Mater. Res. Bull.*, 1987, **22**, 373-380.
32 C. Yang, X. Wang and M. A. Omary, *Angew. Chem. Int. Ed.,* 2009, **48**, 2500-2505.
33 J. E. Auckett, A. A. Barkhordarian, S. H. Ogilvie, S. G. Duyker, H. Chevreau, V. K. Peterson and C. J. Kepert, *Nat. Commun.*, 2018, **9**, 4873.
34 L. Hu, J. Chen, A. Sanson, H. Wu, C. Guglieri Rodriguez, L. Olivi, Y. Ren, L. Fan, J. Deng and X. Xing, *J. Am. Chem. Soc.,* 2016, **138**, 8320-8323.
35 L. Verlet, *Phys. Rev.*, 1967, **159**, 98.
36 A. Sanson, *Chem. Mater.*, 2014, **26**, 3716.
37 F. Bridges, T. Keiber, P. Juhas, S. J. L. Billinge, L. Sutton, J. Wilde and G. R. Kowach, *Phys. Rev. Lett.,* 2014, **112**, 045505.
38 M. G. Tucker, A. L. Goodwin, M. T. Dove, D. A. Keen, S. A. Wells and J. S. Evans, *Phys. Rev. Lett.*, 2005, **95**, 255501.
39 R. West and D. L. Powell, *J. Am. Chem. Soc.*, 1963, **85**, 2577-2579.
40 A. E. Phillips, A. L. Goodwin, G. J. Halder, P. D. Southon and C. J. Kepert, *Angew. Chem. Int. Ed.,* 2008, **120**, 1418-1421.
41 T. R. Ravindran, A. K. Arora and T. A. Mary, *Phys. Rev. Lett.,* 2000, **84**, 3879.
42 D. Yoon, Y. Son, H. Cheong, *Nano Lett.,* 2011, **11**, 3227-3231.
43 C. W. Li, X. Tang, J. A. Munoz, J. B. Keith, S. J. Tracy, D. L. Abernathy and B. Fultz, *Phys. Rev. Lett.*, 2011, **107**, 195504.
44 A. Sanson, M. Giarola, G. Mariotto, L. Hu, J. Chen, X. Xing, *Mater. Chem. Phys.*, 2016, **180**, 213-218.